Supplementary Information

For

An Integrated Magnetic–Microfluidic Chemiluminescence Platform for Rapid Quantification of Exosomal miR-21 Associated with Breast Cancer

This Supplementary Information offers detailed nanoparticle characterization, hydrodynamic simulations, optimization studies, and supporting analytical data that complement the results presented in the main manuscript. These data are provided to keep the main text clear and focused while ensuring transparency, reproducibility, and technical completeness.

Figure S1. FTIR characterization of magnetic nanoparticles

The Fe–O stretching vibration at 562 cm^{-1} confirms the formation of Fe_3O_4. The appearance of Si–O–Si bands at 1097 cm^{-1} indicates successful silica coating. Peaks corresponding to N–H and C–H vibrations confirm APTES modification, while characteristic aldehyde (1719 cm^{-1}) and imine (C=N, 1677 cm^{-1}) peaks verify glutaraldehyde functionalization.

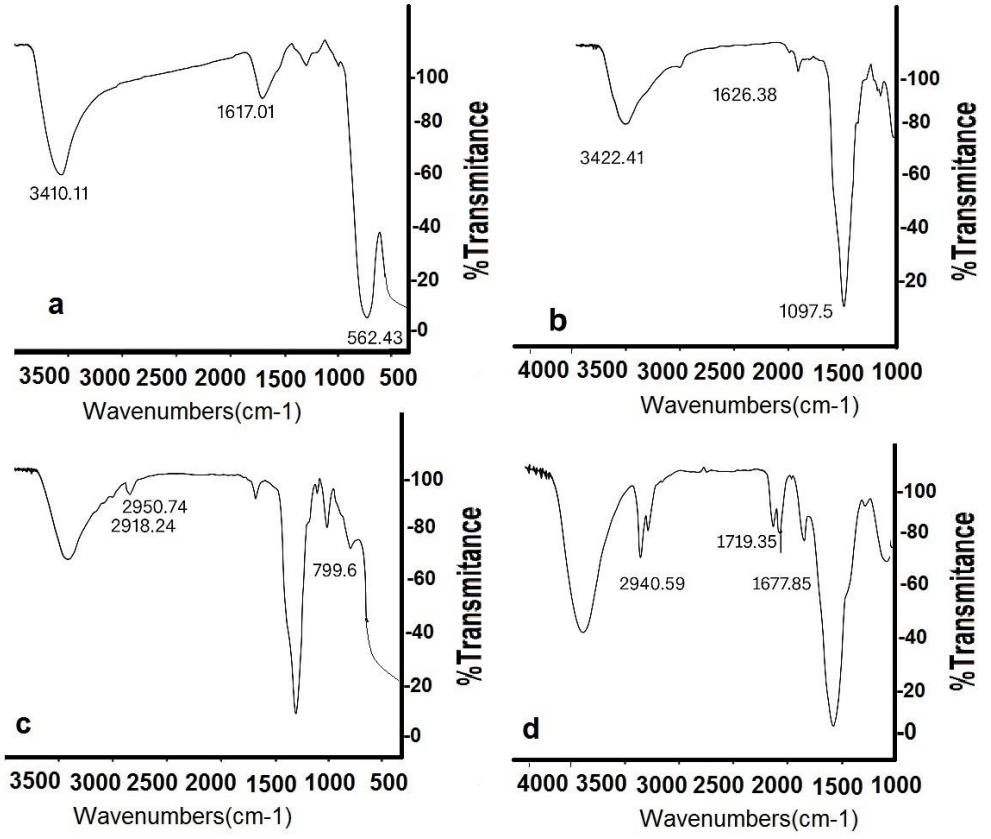

Figure S1. FTIR spectra of Fe_3O_4, Fe_3O_4@SiO_2, Fe_3O_4@SiO_2@APTES, and Fe_3O_4@SiO_2@APTES@glutaraldehyde nanoparticles, confirming stepwise surface functionalization. The Fe–O band (~562 cm^{-1}), Si–O–Si band (~1097 cm^{-1}), and characteristic N–H, C–H, C=O, and C=N vibrations verify successful silica coating, amination, and glutaraldehyde activation.

Figure S2. EDAX analysis of functionalized magnetic nanoparticle

Energy-dispersive X-ray spectroscopy (EDAX) spectra showing the elemental composition of Fe_3O_4@SiO_2@APTES@glutaraldehyde nanoparticles. The presence of Fe, O, Si, C, and N confirms successful silica coating and subsequent amine and aldehyde functionalization.

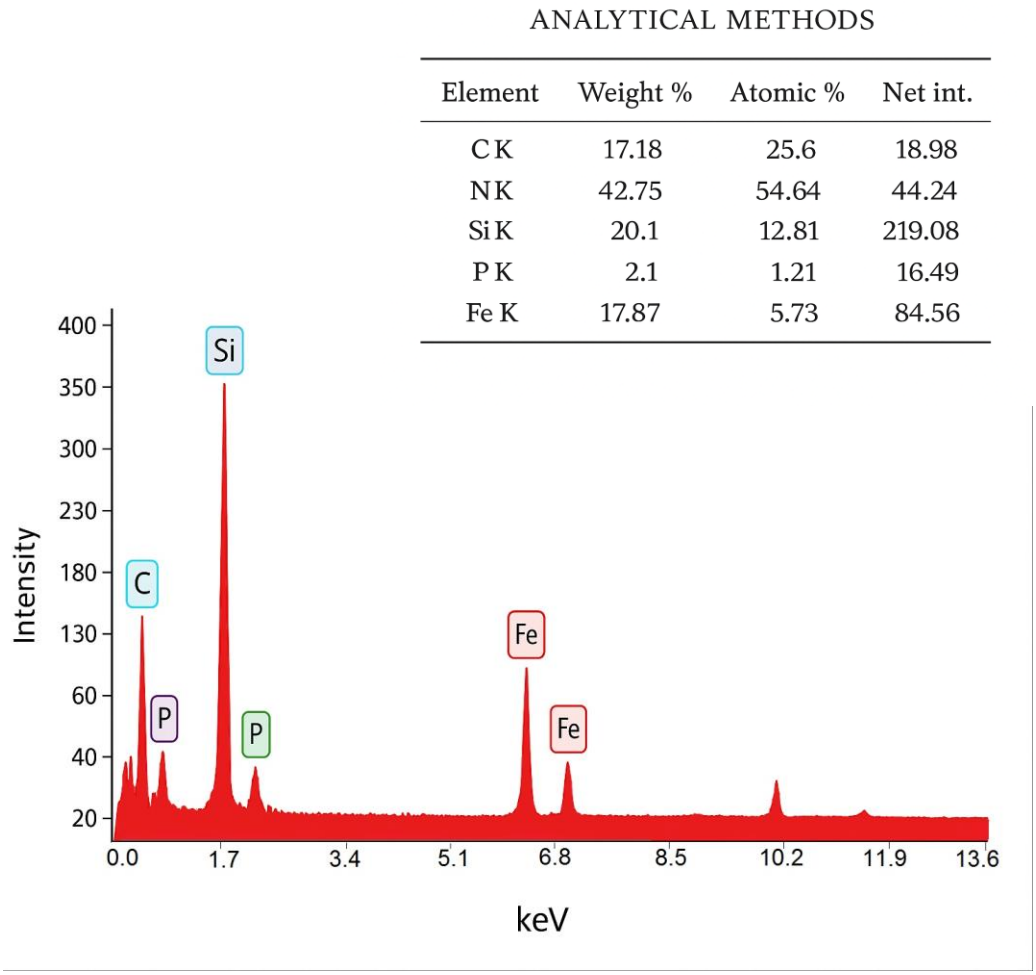

Figure S2. EDAX spectrum of Fe_3O_4@SiO_2@APTES@glutaraldehyde magnetic nanoparticles showing the presence of Fe, O, Si, C, and N, confirming successful silica coating and subsequent surface functionalization.

Figure S3. DLS analysis of magnetic nanoparticles

Dynamic light scattering (DLS) measurements showed a hydrodynamic diameter of approximately 121 nm with a polydispersity index (PDI) of 0.1, indicating uniform size distribution and good colloidal stability of the functionalized nanoparticles in aqueous solution.

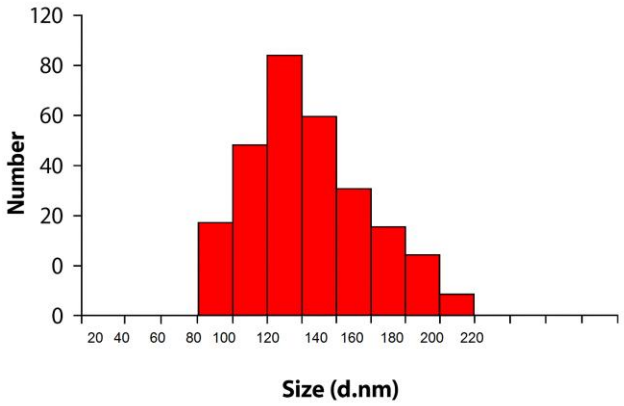

Figure S3. DLS analysis of magnetic nanoparticles showing a hydrodynamic diameter of approximately 121 nm with a narrow size distribution, indicating good colloidal stability.

Figure S4. XRD patterns of magnetic nanoparticles

Zeta potential measurements illustrating surface charge evolution during nanoparticle modification. The shift from negative to positive potential after APTES modification confirms amine group introduction, while subsequent changes after glutaraldehyde activation and probe immobilization reflect successful conjugation of nucleic acid probes.

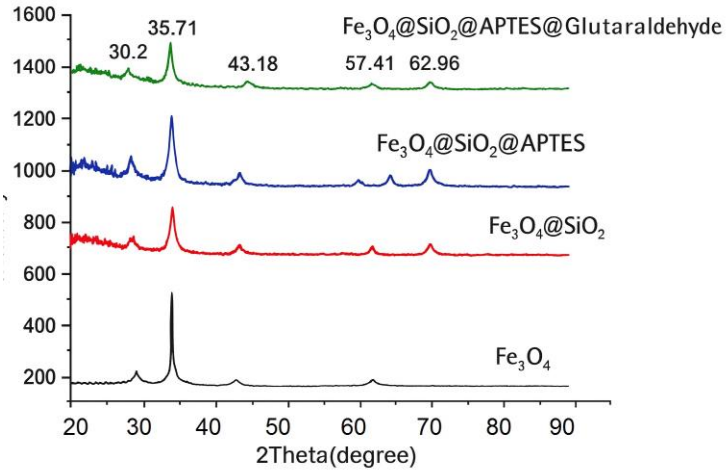

Figure S4. XRD patterns of Fe_3O_4 and surface-modified Fe_3O_4@SiO_2@APTES@glutaraldehyde nanoparticles showing characteristic diffraction peaks of cubic spinel Fe_3O_4, indicating that the crystalline structure is preserved after surface functionalization.

Figure S5. Zeta potential

Zeta potential measurements were performed to monitor surface charge variations during the stepwise functionalization of magnetic nanoparticles. Bare Fe_3O_4 nanoparticles exhibited a negative surface charge (−18.1 mV), which became more negative after silica coating (−31.3 mV) due to surface silanol groups. Subsequent modification with APTES reversed the surface charge to +30.3 mV, confirming the successful introduction of amine functionalities. Glutaraldehyde activation led to a decrease in zeta potential (−44.8 mV), reflecting the presence of aldehyde groups on the surface. After immobilization of the capture probe, the zeta potential shifted to −4.13 mV, consistent with the incorporation of negatively charged phosphate groups from nucleic acids.

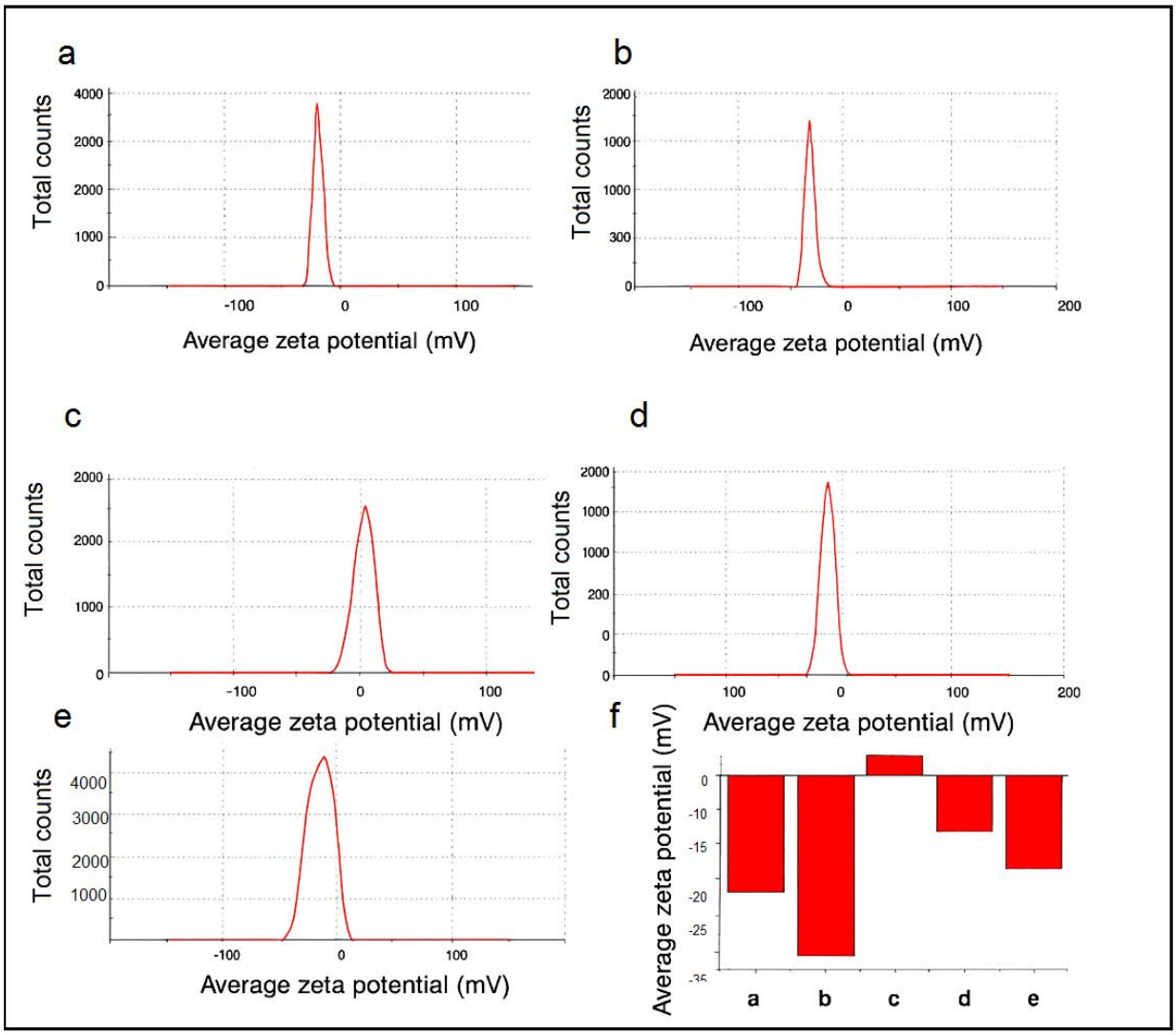

Figure S5. Zeta potential distributions of magnetic nanoparticles during stepwise surface functionalization: (a) bare Fe_3O_4, (b) Fe_3O_4@SiO_2, (c) Fe_3O_4@SiO_2@APTES, (d) Fe_3O_4@SiO_2@APTES@glutaraldehyde, and (e) capture probe–functionalized nanoparticles. Panel (f) summarizes the average zeta potential values, illustrating systematic surface charge changes confirming successful functionalization at each step.

Figure S6. Optimization of analytical parameters

Optimization studies evaluating the effects of key experimental parameters on chemiluminescence (CL) signal intensity, including:

- Detection probe concentration
- Capture probe–functionalized magnetic nanoparticle concentration
- Hybridization time
- Hybridization temperature
- Washing volume and number of washing cycles
- Streptavidin–HRP concentration
- HRP reaction time
- Blocking conditions (BSA concentration and incubation time)

All experiments were performed in triplicate (n = 3). Error bars represent standard deviations. Optimal conditions were selected based on maximum signal intensity and signal-to-noise ratio.

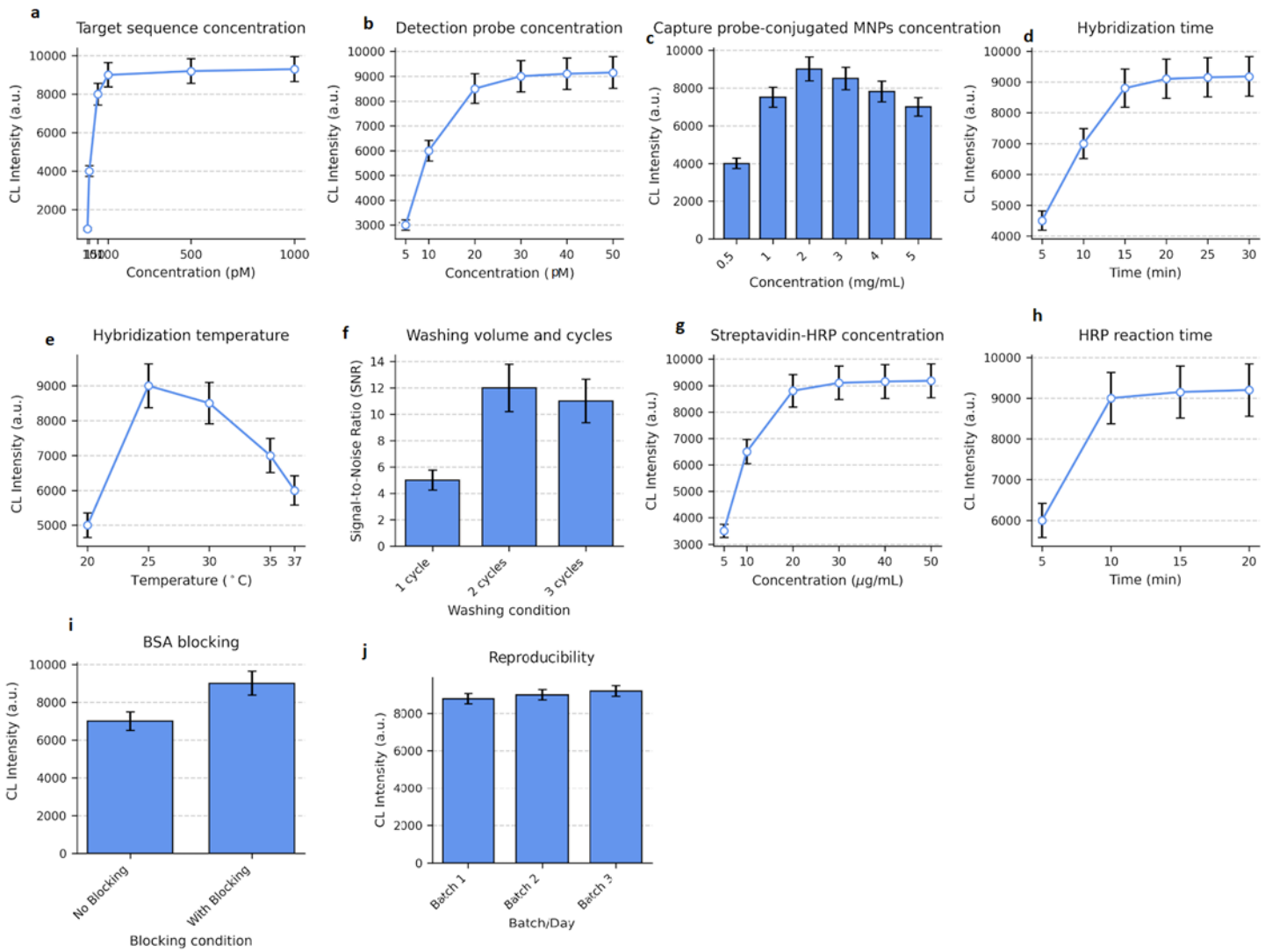

Figure S 6.Optimization of experimental parameters affecting chemiluminescence (CL) signal intensity in the integrated magnetic–microfluidic platform. (a) Effect of target miR-21 concentration. (b) Effect of detection probe concentration. (c) Effect of capture probe–conjugated magnetic nanoparticle (MNP) concentration. (d) Effect of hybridization time. (e) Effect of hybridization temperature. (f) Effect of washing volume and number of washing cycles on signal-to-noise ratio (SNR). (g) Effect of streptavidin–HRP concentration. (h) Effect of HRP reaction time. (i) Effect of BSA blocking on background suppression. (j) Reproducibility of CL signal across different batches/days. All measurements were performed in triplicate (n = 3), and error bars represent standard deviations. Optimal conditions were selected based on maximum CL intensity and improved signal-to-noise ratio.

The following figures and tables provide detailed analyses of nanoparticle physicochemical stability and microfluidic chip performance, which support the system-level accelerated stability results presented in the main manuscript. These stability results support the practical applicability of the platform for point-of-care and translational studies, where reagent robustness under non-ideal storage conditions is critical.

Figure S7. Thermal stability of functionalized magnetic nanoparticles under accelerated storage

Evolution of hydrodynamic diameter and polydispersity index of magnetic nanoparticles stored at 45 °C as a function of time. Data represent mean ± SD (n = 3).

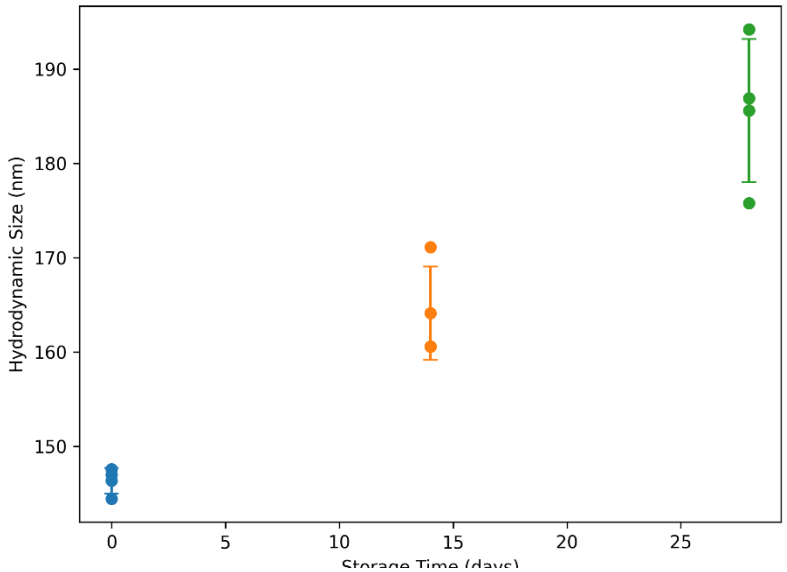

Figure S7. Thermal stability of functionalized magnetic nanoparticles under accelerated storage. Changes in hydrodynamic diameter and polydispersity index of magnetic nanoparticles during storage at 45 °C. Data represent mean ± SD (n = 3).

Figure S8. Surface charge variation of magnetic nanoparticles during accelerated thermal aging

Zeta potential of functionalized magnetic nanoparticles measured at different storage times under accelerated conditions (45 °C). Data represent mean ± SD (n = 3).

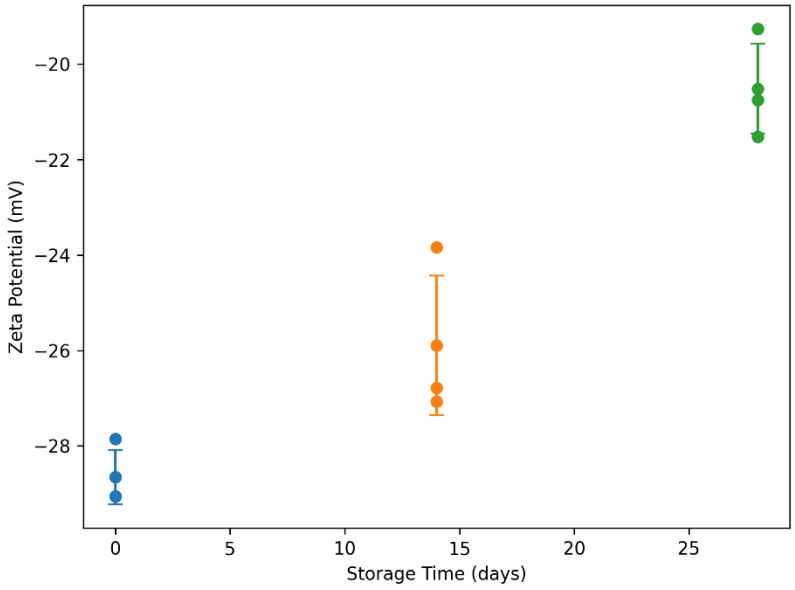

Figure S8. Surface charge evolution of magnetic nanoparticles during accelerated thermal aging. Zeta potential of functionalized magnetic nanoparticles measured as a function of storage time at 45 °C. Data represent mean ± SD (n = 3).

Figure S9. Effect of accelerated thermal storage on target capture efficiency.

Capture efficiency of the functionalized magnetic nanoparticles evaluated using a fixed target concentration after storage at 45 °C. Data represent mean ± SD (n = 3).

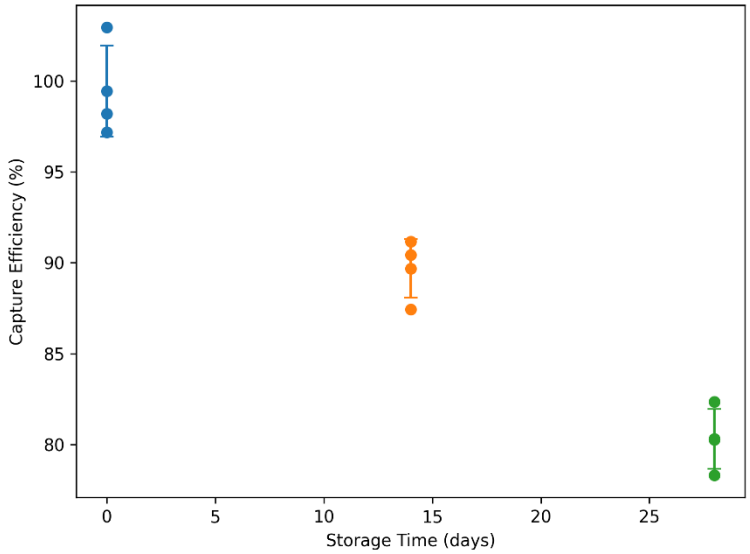

Figure S9. **Effect of accelerated thermal storage on target capture efficiency.** Capture efficiency of capture probe–functionalized magnetic nanoparticles evaluated using a fixed miR-21 target concentration after storage at 45 °C for different time intervals. The retained capture performance indicates that the surface-immobilized probes remain functionally active under accelerated aging conditions. Data are presented as mean ± SD (n = 3).

Supplementary Methods

1. Calculation of probe surface coverage

The surface loading and coverage of the amine-terminated capture probe immobilized on Fe_3O_4@SiO_2@APTES@glutaraldehyde magnetic nanoparticles were quantitatively determined using a UV–Vis depletion method combined with hydrodynamic size measurements (DLS) and geometric modeling. This approach enables estimation of (i) probe loading capacity (pmol mg^{-1}), (ii) number of probes per nanoparticle, and (iii) surface coverage expressed as probes per unit surface area (probes nm^{-2}).

Step1. Determination of immobilized probe amount by UV–Vis depletion

A known concentration of amine-modified capture probe was incubated with a known mass of aldehyde-activated magnetic nanoparticles under the conjugation conditions described in the Materials and Methods section. Following conjugation, the nanoparticles were magnetically separated, and the absorbance of the supernatant was measured at 260 nm to quantify the concentration of unbound probe.

The concentration of free probe in the supernatant was calculated using either a calibration curve or the Beer–Lambert law:

$A260 = \varepsilon 260 \times l \times C$

The amount of probe immobilized on the nanoparticle surface was obtained by depletion:

$nbound = (C0 - Cf) \times V$

The probe loading capacity was calculated as:

$L = nbound / MNP$

Based on the experimental depletion measurements, the probe loading capacity was determined to be approximately 90 pmol mg^{-1}.

Step2. Estimation of the number of probes per nanoparticle

The number of probe molecules immobilized per milligram of nanoparticles was calculated as:

$Nprobe/mg = L \times 10^{-12} \times NA$

For a loading capacity of 90 pmol mg^{-1}, this corresponds to approximately 5.4×10^{13} probe molecules per mg of nanoparticles.

The hydrodynamic diameter of the functionalized nanoparticles measured by DLS was approximately 121 nm (radius ≈ 60.5 nm). Assuming spherical geometry, the number of probes per nanoparticle was estimated to be approximately 250.

Step3. Calculation of surface coverage

The surface area of a single nanoparticle was calculated assuming a spherical geometry:

$ANP = 4\pi r^2$

Using r = 60.5 nm, the surface area was calculated to be approximately 4.6×10^4 nm^2.

Surface coverage (Γ) was calculated as:

$\Gamma = Nprobe/NP / ANP$

This yields a surface coverage of approximately 5.5×10^{-3} probes nm^{-2}.

Assumptions and considerations

1. The nanoparticle diameter used in calculations was obtained from DLS measurements and therefore represents the hydrodynamic diameter.
2. Complete magnetic separation of nanoparticles was assumed during UV–Vis depletion measurements.
3. Surface coverage values fall within the typical range reported for DNA-functionalized magnetic nanoparticles.

Supplementary Discussion

The data presented in this Supplementary Information provide essential technical validation of nanoparticle functionalization, microfluidic performance, and assay robustness. These results support the reproducibility and practical applicability of the integrated platform while allowing the main manuscript to remain focused on the core analytical findings.